2015 IEEE/RSJ International Conference on Intelligent Robots and Systems (IROS)
Congress Center Hamburg
Sept 28 - Oct 2, 2015. Hamburg, Germany

On Modeling and Control of a Holonomic Vectoring Tricopter

Michalis Ramp[1] and Evangelos Papadopoulos[2], *Senior Member, IEEE*

***Abstract*— The modeling and control of a vectoring tricopter UAV are developed in this article. The UAV is actuated by three thrust motors, each guided by suitable actuators, thus forming a platform able to independently track any desired attitude and trajectory. The derivation of the equations of motion is followed by the development of a vectoring controller that is supplemented by an allocation strategy. Both are based on geometric feedback linearization techniques, resulting in a singularity-free control law, taking into account the inertia effects of the main body, of the motors, and of the vectoring dynamics (actuators). A stability proof is developed validating the effectiveness of the control strategy under bounded disturbances. Simulations showcase the developed controller and tricopter performance.**

I. INTRODUCTION

Advances during the last decade in sensors, materials, electronics and power sources made the construction of small scale UAVs feasible, and resulted in a wave of research in this area. Small scale UAVs have a variety of industrial and military applications ranging from aerial photography, inspection and mapping, to surveillance and security. Substantial work has been devoted in quadrotor UAVs due to their simple construction and mechanics, resulting in vehicles able to perform aggressive and cooperative maneuvers, and grasping and transportation of objects [1],[2].

Although initial quadrotor designs were subject to axes coupling, currently the development of UAVs with independent axis control is given high priority since such capabilities can extend the use of UAVs as versatile field robots [3],[4],[5],[6]. Indeed, a UAV underactuated (uUAV) with respect to the main body degrees-of-freedom (dof), must tilt its body in order to move sideways limiting its ability to attain the proper pose that would allow it to traverse cluttered spaces. For inspection/surveillance tasks, uUAVs need a supplementary apparatus like controllable/actuated camera mounts along with elaborate path planing trajectories, so that the transmitted camera image can be kept level and not tire an operator. More difficult physical interaction tasks, such as force/torque application in arbitrary directions or assembly tasks cannot be performed by a uUAV but instead are only possible under some very specific conditions [2].

In contrast to a uUAV, a holonomic vehicle with independent axes control can vary independently its position and attitude, forming a true six dof robotic platform, capable for any inspection/surveillance task, for traversing cluttered space, and for assembly or interaction tasks, with no external apparatuses, keeping at the same time the overall size small.

Towards this direction, a UAV having *eight* rotors (quadrotor with four side rotors) was proposed aiming to decouple the attitude/translational dynamics [3]. However, the independent translational/attitude dynamics were restricted to a narrow envelope of the orientation. A *hexrotor* design with complete control over its trajectory/attitude was proposed in [4], and in [5] where the UAV has variable pitch propellers. However, the fixed orientation of the canted rotors results in poor maneuverability at some attitudes. A *quadrotor* with four tilting propellers independently spanning both the E^3 and $SO(3)$ spaces was proposed in [6]. This design still utilizes four thrusting rotors.

In view of the above, this work is motivated by the need to design a vehicle with independent axes control and with a small number of thrusting motors. Its focus is the development of a holonomic vehicle using only three vectored thrusting motors, i.e. less than those in [3],[4],[5],[6], and a computationally inexpensive control strategy that will not be susceptible to singular configurations, resulting in a UAV with decoupled translational/attitude response. The derivation of the equations of motion is done using a Newton-Euler approach that allows display of the internal forces and torques between the thrusting motors and their base. A geometric allocation strategy based on the complete multibody dynamics, and a geometric vectoring controller are developed and result in a singularity-free control law. This control law takes into account the full system dynamics, including the inertia effects of the main body, of the thrusting motors and of the vectoring actuators, and remains effective in the presence of modeling inaccuracies. It is shown by a stability proof that the control law results in a uniformly ultimately bounded system under bounded disturbances. Simulation results validate the developed controller and showcase responses characterized by independent motion in six dimensions.

II. DYNAMICS

A. Description and definitions. The vectoring tricopter UAV is comprised of three thrusting motors located at the extremities of the UAV's three legs (see Fig. 1); each guided by suitable actuators capable to point each thrusting motor. The legs are coplanar with an 120^o axial offset. The tricopter frame is chosen on overall cost considerations. The frame is simple in construction, requires less materials and is also lighter in contrast to a quad/hexarotor frame that has to support more motors. Furthermore its geometry allows for flexibility in placing payloads, such as a camera, closer to

[1]M. Ramp is with the Department of Mechanical Engineering, National Technical University of Athens, (NTUA) 15780 Athens, Greece rampmich@mail.ntua.gr

[2]E. Papadopoulos is with the Department of Mechanical Engineering, NTUA, 15780 Athens (tel: +30-210-772-1440; fax: +30-210-772-1455) egpapado@central.ntua.gr

978-1-4799-9993-4/15/$31.00 ©2015 IEEE

the center of mass (CM) due to the 120^o offset between the tricopter legs.

The vectoring definition implies that each motor will be pointed in S^2, i.e. the unit sphere in the three dimensional space. The actuator assembly together with the i^{th} motor/propeller comprises the vectoring apparatus (VA) (see Fig. 1) that generates a thrusting force/gyroscopic moment on leg i. An inertial reference frame $\mathbf{I}_R\{\mathbf{E}_1, \mathbf{E}_2, \mathbf{E}_3\}$ and a base-fixed frame $\mathbf{I}_b\{\mathbf{e}_1, \mathbf{e}_2, \mathbf{e}_3\}$ at the base center of mass (CM) are chosen, together with three i^{th} motor-fixed frames $\mathbf{I}_i\{\mathbf{e}_{i,1}, \mathbf{e}_{i,2}, \mathbf{e}_{i,3}\}$ where i = 1,2,3 denotes the i^{th}-VA.

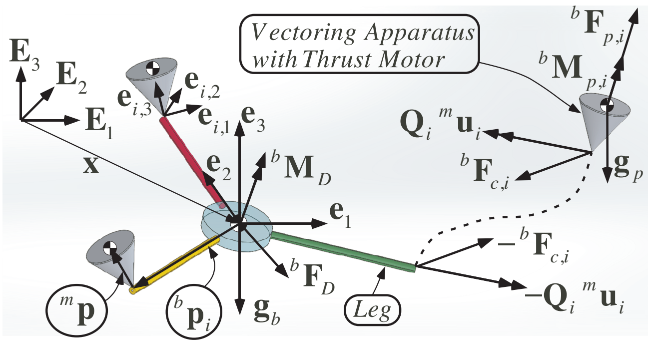

Fig. 1. Free-body diagram (FBD) of the Vectoring Tricopter concept with the coordinate frames, forces, moments and vectors that define it.

TABLE I. Definitions

Right Subscript	
$(.)_i$	i^{th}-VA number
$(.)_d$	Desired rotation matrix/vector/signal
Left superscript	
${}^b(.)$	Vector expressed in base fixed frame $\mathbf{I}_b$
${}^m(.)_i$	Vector expressed in i^{th}motor-fixed frame, $\mathbf{I}_i$
Definitions	
$\mathbf{x}, \mathbf{x}_i \in \mathbf{R}^3$	Position of the base, i^{th}-VA wrt $\mathbf{I}_R$ in $\mathbf{I}_R$
$\mathbf{v}, \mathbf{v}_i \in \mathbf{R}^3$	Velocity of the base, i^{th}-VA wrt $\mathbf{I}_R$ in $\mathbf{I}_R$
${}^b\boldsymbol{\omega} \in \mathbf{R}^3$	Angular velocity of the base wrt $\mathbf{I}_R$ in $\mathbf{I}_b$
${}^m\boldsymbol{\omega}_i \in \mathbf{R}^3$	Angular velocity, i^{th}-VA wrt $\mathbf{I}_R$ in $\mathbf{I}_i$
${}^m\boldsymbol{\omega}_i^r \in \mathbf{R}^3$	Angular velocity, i^{th}-VA wrt $\mathbf{I}_b$ in $\mathbf{I}_i$
$\mathbf{Q} \in$ SO (3)	Rotation matrix from $\mathbf{I}_b$ to $\mathbf{I}_R$ frame
$\mathbf{Q}_i \in$ SO (3)	Rotation matrix from $\mathbf{I}_i$ to $\mathbf{I}_b$ frame
${}^m\mathbf{u}_i \in \mathbf{R}^3$	Control torque applied on i^{th}-VA in $\mathbf{I}_i$
$b_F, b_T \in \mathbf{R}$	Force and Torque constants
$g, \rho \in \mathbf{R}$	Gravity and Air density constants
${}^m\mathbf{p} \in \mathbf{R}^3$	Vector connecting the extremity of Leg i with the CM of the i^{th}-VA in $\mathbf{I}_i$
${}^b\mathbf{q}_i \in \mathbf{R}^3$	Unit vector, co-linear to the i^{th} propeller axis, equal to $\mathbf{Q}_i({}^m\mathbf{p}/\|{}^m\mathbf{p}\|)$ in $\mathbf{I}_b$
${}^b\mathbf{p}_i \in \mathbf{R}^3$	Vector connecting the CM of the base with the extremity of Leg i in $\mathbf{I}_b$
$f_i \in \mathbf{R}$	Force component of the i^{th}-VA in the $\{\mathbf{e}_{i,3}\}$ direction equal to $b_F\,({}^m\boldsymbol{\omega}_i \cdot \mathbf{e}_{i,3})^2$ [10]
$\mathbf{J} \in \mathbf{R}^{3\times3}$	Inertial matrix (IM) of the base in $\mathbf{I}_b$
$\mathbf{J}_p \in \mathbf{R}^{3\times3}$	IM of i^{th}-VA in $\mathbf{I}_i$
$m \in \mathbf{R}$	Total UAV mass $(m_b + 3m_p)$ where m_b: mass of the frame and m_p: mass of a VA
$\mathbf{g}_p \in \mathbf{R}^3$	Gravity force $(-m_p g\mathbf{E}_3)$ on VA, in $\mathbf{I}_R$
$\mathbf{g}_b \in \mathbf{R}^3$	Gravity force $(-m_b g\mathbf{E}_3)$ on base, in $\mathbf{I}_R$
$\mathbf{g}_S \in \mathbf{R}^3$	Total gravity force $(\mathbf{g}_b + 3\mathbf{g}_p)$ on UAV
${}^b\mathbf{F}_D \in \mathbf{R}^3$	Wind disturbance force in $\mathbf{I}_b$ [11]
${}^b\mathbf{M}_D \in \mathbf{R}^3$	Wind disturbance moment in $\mathbf{I}_b$ [11]

Note that if the left superscript of a vector is omitted, then the vector is expressed in $\mathbf{I}_R$. The VA is modeled as a rigid body attached on leg i, see Fig. 1. During pointing the VA and simultaneously maintaining a desired propeller speed about the pointing direction, a force $f_i\mathbf{e}_{i,3}$ [10] and a torque $b_T f_i \mathbf{e}_{i,3}$ [1] are generated. Thus the third component of the control torque ${}^m\mathbf{u}_i$ is the torque of the i^{th} thrusting propeller while the first two components are required to point the i^{th} motor. Finally the UAV configuration is defined by the location of its base CM, $\mathbf{x}$ and base attitude, $\mathbf{Q}$ together with the attitude of the three VA's, $\mathbf{Q}_i$, i=1,2,3. The configuration manifold is $\mathbf{G}$ =SE(3)×SO(3)×SO(3)×SO(3).

B. Kinetics. The Newton-Euler methodology is employed for the derivation of the UAV equations of motion. The position of the CM of the i^{th}-VA is,

$$ {}^b\mathbf{x}_i = \mathbf{Q}^T\mathbf{x}_i, \mathbf{x}_i = \mathbf{x} + \mathbf{Q}({}^b\mathbf{p}_i + \mathbf{Q}_i\,{}^m\mathbf{p}) $$

The i^{th}-*vectoring apparatus* dynamics are described by,

$$ {}^b\dot{\mathbf{x}}_i = {}^b\mathbf{v}_i $$

$$ m_p\,{}^b\dot{\mathbf{v}}_i = {}^b\mathbf{F}_{p,i} + {}^b\mathbf{F}_{c,i} + \mathbf{Q}^T\mathbf{g}_p \tag{1a} $$

$$ \mathbf{J}_p\,{}^m\dot{\boldsymbol{\omega}}_i + {}^m\boldsymbol{\omega}_i \times \mathbf{J}_p\,{}^m\boldsymbol{\omega}_i = {}^m\mathbf{u}_i + \mathbf{Q}_i^T({}^b\mathbf{M}_{c,i} + {}^b\mathbf{M}_{p,i}) \tag{1b} $$

$$ \dot{\mathbf{Q}}_i = \mathbf{Q}_i S({}^m\boldsymbol{\omega}_i) \tag{1c} $$

where ${}^b\mathbf{F}_{p,i}$, ${}^b\mathbf{M}_{p,i}$ is the thrust force and torque generated by the i^{th} thrusting motor,

$$ {}^b\mathbf{F}_{p,i} = \mathbf{Q}_i(f_i\mathbf{e}_{i,3}) = \mathbf{Q}_i[0; 0; f_i],\ {}^b\mathbf{M}_{p,i} = b_T\,{}^b\mathbf{F}_{p,i} \tag{2} $$

The ${}^b\mathbf{F}_{c,i}$, ${}^b\mathbf{M}_{c,i}$ are forces and resulting moments applied on the i^{th}-VA by the base and given by,

$$ {}^b\mathbf{F}_{c,i} = m_p\,{}^b\dot{\mathbf{v}}_i - \mathbf{Q}^T\mathbf{g}_p - {}^b\mathbf{F}_{p,i} \tag{3a} $$

$$ {}^b\mathbf{M}_{c,i} = (\mathbf{Q}_i(-{}^m\mathbf{p})) \times {}^b\mathbf{F}_{c,i},\ {}^m\mathbf{p} = d\mathbf{e}_{i,3} = [0; 0; d] \tag{3b} $$

The cross product mappings $S()$, $S^{-1}()$, the accelerations, and the angular velocities are defined in the Appendix.

Having the dynamic equations of the VA, the equations for the translational and attitude dynamics of the UAV can now be derived. Following the Newton-Euler methodology, for the translational dynamics, see "Leg" in Fig. 1, the motion can be described by the tricopter frame/base dynamics under the influence of the forces $-{}^b\mathbf{F}_{c,i}$ generated by each VA (calculated by (1a)) and the body-exerted gravity force $\mathbf{g}_b$. Moment-wise (see "Leg" in Fig. 1) each VA exerts a moment $-{}^m\mathbf{u}_i$, on the base. Then, the *base* dynamics are given by,

$$ \dot{\mathbf{x}} = \mathbf{v} $$

$$ m_b\dot{\mathbf{v}} = \mathbf{g}_b + \mathbf{Q}({}^b\mathbf{F}_D - \sum_{i=1}^{3} {}^b\mathbf{F}_{c,i}) \tag{4a} $$

$$ \mathbf{J}^b\dot{\boldsymbol{\omega}} = \sum_{i=1}^{3}\Big(-\mathbf{Q}_i\,{}^m\mathbf{u}_i + {}^b\mathbf{p}_i \times (-{}^b\mathbf{F}_{c,i})\Big) + {}^b\mathbf{M}_D - {}^b\boldsymbol{\omega} \times \mathbf{J}^b\boldsymbol{\omega} \tag{4b} $$

$$ \dot{\mathbf{Q}} = \mathbf{Q}S({}^b\boldsymbol{\omega}) \tag{4c} $$

The disturbance wrench $[{}^b\mathbf{F}_D; {}^b\mathbf{M}_D]$, simulating the wind is assumed to be bounded and is modeled as in [11]. The inputs for the equations above are the pointing moments ${}^m\mathbf{u}_i$ (i=1,2,3) that actuate the i^{th}-VA, pointing it in space while producing the motor generated thrust forces ${}^b\mathbf{F}_{p,i}$ and moments ${}^b\mathbf{M}_{p,i}$. Note that the equations of motion are highly coupled. This can be seen by rewriting the equations in matrix form with respect to $[\dot{\mathbf{v}};{}^b\dot{\boldsymbol{\omega}};{}^m\dot{\boldsymbol{\omega}}_1;{}^m\dot{\boldsymbol{\omega}}_2;{}^m\dot{\boldsymbol{\omega}}_3]$,

$$\mathbb{M}(\mathbf{Q},\mathbf{Q}_1,\mathbf{Q}_2,\mathbf{Q}_3)\begin{bmatrix}\dot{\mathbf{v}}\\ {}^b\dot{\boldsymbol{\omega}}\\ {}^m\dot{\boldsymbol{\omega}}_1\\ {}^m\dot{\boldsymbol{\omega}}_2\\ {}^m\dot{\boldsymbol{\omega}}_3\end{bmatrix}+\begin{bmatrix}\mathbf{Q}(\sum_{i=1}^3\Phi_i-\Delta)\\ \mathrm{E}\\ \Gamma_1\\ \Gamma_2\\ \Gamma_3\end{bmatrix}=\mathbf{U} \quad (5)$$

$$\dot{\mathbf{Q}}=\mathbf{Q}S({}^b\boldsymbol{\omega}),\dot{\mathbf{Q}}_i=\mathbf{Q}_iS({}^m\boldsymbol{\omega}_i),i=1,2,3$$

where $\mathbb{M}\in\mathbb{R}^{15\times15}$ see (A5) in the last page and,

$$\mathbf{U}=[0;\sum_{i=1}^3(-\mathbf{Q}_i{}^m\mathbf{u}_i);{}^m\mathbf{u}_1;{}^m\mathbf{u}_2;{}^m\mathbf{u}_3]$$

$$\Phi_i={}^b\boldsymbol{\omega}\times({}^b\boldsymbol{\omega}\times({}^b\mathbf{p}_i+\mathbf{Q}_i{}^m\mathbf{p}))+2({}^b\boldsymbol{\omega}\times\mathbf{Q}_i({}^m\boldsymbol{\omega}_i\times{}^m\mathbf{p}))$$
$$+\mathbf{Q}_i({}^m\boldsymbol{\omega}_i\times({}^m\boldsymbol{\omega}_i\times{}^m\mathbf{p}))$$

$$\Delta=\mathbf{g}_b+\mathbf{Q}({}^b\mathbf{F}_D+\sum_{i=1}^3({}^b\mathbf{F}_{p,i}+\mathbf{Q}^T\mathbf{g}_p))$$

$$\mathrm{E}=\sum_{i=1}^3S({}^b\mathbf{p}_i)m_p\Phi_i-{}^b\mathbf{p}_i\times(\mathbf{Q}^T\mathbf{g}_p+{}^b\mathbf{F}_{p,i}))$$
$$+{}^b\boldsymbol{\omega}\times\mathbf{J}^b\boldsymbol{\omega}-{}^b\mathbf{M}_D$$

$$\Gamma_i={}^m\boldsymbol{\omega}_i\times\mathbf{J}_p{}^m\boldsymbol{\omega}_i-\mathbf{Q}_i^TS(\mathbf{Q}_i(-{}^m\mathbf{p}))m_p\Phi_i-\mathrm{B}_i$$

$$\mathrm{B}_i=\mathbf{Q}_i^T[{}^b\mathbf{M}_{p,i}-(\mathbf{Q}_i(-{}^m\mathbf{p}))\times(\mathbf{Q}^T\mathbf{g}_p+{}^b\mathbf{F}_{p,i})]$$

The equations of motion of the entire UAV are given by (1-4), or in matrix form by (5).

III. CONTROL DESIGN

Since the goal is the design of a holonomic vehicle able to track arbitrary poses, a suitable controller is needed with an almost global operational envelope. This condition guides us to employ geometric control techniques as they are singularity free and simplify the control design [7],[8],[9],[14]. First we propose a geometric thrust allocation strategy that produces the reference pointing directions and propeller velocities for each VA so that the base is able to track a desired pose. Then we design a controller able to *point* each VA with respect to the base, while simultaneously actuating the VA's propeller to the *desired speed*. This task is carried out assuming that the forces and moments transmitted by the VA's to the base can be estimated approximately using sensors and/or computationally, allowing us to treat the VA's as separate systems. Finally a stability proof is developed showing that with the developed controller, the vehicle exhibits holonomic response tracking a desired pose under bounded disturbances.

A. Allocation strategy. We develop a tricopter thrust allocation strategy, using the attitude error function $\Psi(\mathbf{Q},\mathbf{Q_d})$, see (A1). This attitude error function compares the current attitude as it is encapsulated in $\mathbf{Q}$ with the desired attitude given by $\mathbf{Q}_d$. If $\mathbf{Q}$ is antipodal to $\mathbf{Q}_d$, using (A1) then Ψ=2, translating to the maximum attitude difference of 180^o with respect to an equivalent axis angle rotation. If $\mathbf{Q}$=$\mathbf{Q}_d$ then Ψ=0 signifying the same attitude. This attitude error function yields the attitude/angular velocity errors defined as in [8],

$$\mathbf{e}_{\mathbf{x},\mathbf{Q}}=\begin{bmatrix}\mathbf{e}_x\\ \mathbf{e}_Q\end{bmatrix}=\begin{bmatrix}\mathbf{x}-\mathbf{x}_d\\ \frac{1}{2\sqrt{1+tr[\mathbf{Q}_d^T\mathbf{Q}]}}S^{-1}\left(\mathbf{Q}_d^T\mathbf{Q}-\mathbf{Q}^T\mathbf{Q}_d\right)\end{bmatrix} \quad (6)$$

$$\mathbf{e}_{\mathbf{v},\boldsymbol{\omega}}=[\mathbf{e}_v;\mathbf{e}_\omega]=\left[\mathbf{v}-\mathbf{v}_d;\ {}^b\boldsymbol{\omega}-\mathbf{Q}^T\mathbf{Q}_d{}^b\boldsymbol{\omega}_d\right] \quad (7)$$

A necessary condition is that $\mathbf{Q}_d$ is not antipodal to $\mathbf{Q}$ since $\mathbf{e}_Q$ vanishes and the tricopter stays at its current attitude. Using (4a-4b), (1a-1b) and output feedback linearization techniques [13], the desired thrusts are found to be,

$$\begin{bmatrix}{}^b\mathbf{F}_{p,1}\\ {}^b\mathbf{F}_{p,2}\\ {}^b\mathbf{F}_{p,3}\end{bmatrix}_d=\mathbf{A}^\#\begin{bmatrix}\mathbf{Q}^T & \mathbf{0}\\ \mathbf{0} & \mathbf{I}\end{bmatrix}\left(\begin{bmatrix}m_b\dot{\mathbf{v}}_r\\ {}^b\dot{\boldsymbol{\omega}}_r\end{bmatrix}-\begin{bmatrix}\mathbf{g}_S\\ \mathbf{H}\end{bmatrix}\right) \quad (8)$$

where for $c_x,c_2,k_v,k_x,k_\omega,k_\Omega,k_R,k_Q>0$

$$\begin{bmatrix}\dot{\mathbf{v}}_r\\ {}^b\dot{\boldsymbol{\omega}}_r\end{bmatrix}=\begin{bmatrix}\dot{\mathbf{v}}_d-k_v\mathbf{e}_v-c_xk_x\mathbf{e}_x\\ -(k_\omega+k_\Omega)\mathbf{e}_\omega-(k_R+c_2k_Q)\mathbf{e}_Q\end{bmatrix} \quad (9)$$

$$\begin{aligned}\mathbf{H}=&\mathbf{J}^b\boldsymbol{\omega}\times{}^b\boldsymbol{\omega}+\mathbf{J}\left(S({}^b\boldsymbol{\omega})\mathbf{Q}^T\mathbf{Q}_d{}^b\boldsymbol{\omega}_d-\mathbf{Q}^T\mathbf{Q}_d{}^b\dot{\boldsymbol{\omega}}_d\right)\\ &+\sum_{i=1}^3\Big(\mathbf{Q}_i\big(\mathbf{J}_p(S({}^m\boldsymbol{\omega}_i)\mathbf{Q}_i^T\mathbf{Q}_{i,d}{}^m\boldsymbol{\omega}_{i,d}\\ &-\mathbf{Q}_i^T\mathbf{Q}_{i,d}{}^m\dot{\boldsymbol{\omega}}_{i,d})-{}^m\boldsymbol{\omega}_i\times\mathbf{J}_p{}^m\boldsymbol{\omega}_i\big)\\ &+(\mathbf{Q}_i{}^m\mathbf{p}+{}^b\mathbf{p}_i)\times(\mathbf{Q}^T\mathbf{g}_p)\Big)\end{aligned} \quad (10)$$

The matrix $\mathbf{A}$=$[\mathbf{A}_F;\mathbf{A}_M]\in\mathbb{R}^{6\times9}$ has rank equal to six,

$$\mathbf{A}=[\mathbf{I},\mathbf{I},\mathbf{I};b_T\mathbf{I}+S(\mathbf{A}_1),b_T\mathbf{I}+S(\mathbf{A}_2),b_T\mathbf{I}+S(\mathbf{A}_3)]$$

$$\mathbf{A}_{i=1,2,3}=\mathbf{Q}_i{}^m\mathbf{p}+{}^b\mathbf{p}_i$$

and is used to calculate $\mathbf{A}^\#$=$\mathbf{A}^T(\mathbf{A}\mathbf{A}^T)^{-1}\in\mathbb{R}^{9\times6}$ which is the Moore-Penrose pseudoinverse. The reference commands for the propeller direction and speed (${}^b\mathbf{q}_{i,d}$, ${}^m\boldsymbol{\omega}_{i,d}$) are extracted from the desired forces ${}^b\mathbf{F}_{p,i_d}$ as follows:

$${}^m\boldsymbol{\omega}_{i,d}=\sqrt{b_F^{-1}\|{}^b\mathbf{F}_{p,i_d}\|}\mathbf{e}_{i,3}=[0;0;\sqrt{b_F^{-1}\|{}^b\mathbf{F}_{p,i_d}\|}] \quad (11)$$

$${}^b\mathbf{q}_{i,d}={}^b\mathbf{F}_{p,i_d}/\|{}^b\mathbf{F}_{p,i_d}\| \quad (12)$$

Note that for the allocation scheme to be able to produce the reference commands the condition $\|{}^b\mathbf{F}_{p,i_d}\|\neq0$ must hold. This is ensured by the presence of gravity in conjunction to the requirement that the reference trajectories should be sufficiently smooth and three times differentiable with respect to time. In this manner no sudden accelerations appear due to trajectory smoothness and since the gravity must be continuously compensated $\|{}^b\mathbf{F}_{p,i_d}\|\neq0$.

B. Vectoring controller. For the vectoring of each VA, a controller able to *point* each propeller while simultaneously regulating its *speed* is needed. Furthermore, since we develop a holonomic vehicle able to hover and maneuver at any attitude, we require that this controller should be singularity free i.e. geometric, to ensure smooth operation. This leads to a pointing direction/angular velocity stabilization problem, which will be carried out under the assumption that the interaction wrench between the base and each VA is estimated, allowing us to treat each VA as a separate system. We addressed the above problem in [12] where we developed a vectoring controller able to point a rigid body, while simultaneously regulating its speed about the pointing direction using geometric methods. Here we redesign the above controller to the application at hand by using a different error function in order to get stronger tracking for small attitude errors. This is needed since we must be able to track the allocation generated pointing directions/propeller speeds precisely. We will use the attitude error function

$$\Psi_i=1-{}^b\mathbf{q}_i\cdot{}^b\mathbf{q}_{i,d} \quad (13)$$

which was introduced in [7],[9] where the control problem of attitude stabilization to a desired pointing direction while driving the angular velocity to zero was addressed. In [7],[9] Ψ_i yielded ${}^b\mathbf{e}_{q,i}$=${}^b\mathbf{q}_{i,d}\times{}^b\mathbf{q}_i$, ${}^b\mathbf{e}_{\omega,i}$=${}^b\boldsymbol{\omega}_i$ as configuration error vectors. As a result the controller in [7],[9] is subject to the limitation that the angular velocity is driven to zero. Since we track time-varying attitudes and non-zero angular velocities, those configuration errors are unsuitable.

Instead we use Ψ_i as an intermediate step to find ${}^b\mathbf{e}_{q,i}$, ${}^b\mathbf{e}_{\omega,i}$ for time varying ${}^b\mathbf{q}_{i,d}$, ${}^b\boldsymbol{\omega}_{i,d}$ to get ${}^b\mathbf{e}_{q,i}={}^b\mathbf{q}_{i,d}\times{}^b\mathbf{q}_i$, ${}^b\mathbf{e}_{\omega,i}={}^b\boldsymbol{\omega}_i-{}^b\boldsymbol{\omega}_{i,d}$. Note that in the intermediate angular velocity error ${}^b\mathbf{e}_{\omega,i}$, both ${}^b\boldsymbol{\omega}_i$ and ${}^b\boldsymbol{\omega}_{i,d}$ lie on different tangent spaces. To correct this, we transform the intermediate error vectors in $\mathbf{I}_i$ to derive the final form of the i^{th}-VA configuration errors as,

$$
\begin{aligned}
{}^m\mathbf{e}_{q,i} &= \mathbf{Q}_i^T\left({}^b\mathbf{q}_{i,d}\times{}^b\mathbf{q}_i\right) && (14)\\
{}^m\mathbf{e}_{\boldsymbol{\omega},i} &= \mathbf{Q}_i^T({}^b\boldsymbol{\omega}_i-{}^b\boldsymbol{\omega}_{i,d}) = {}^m\boldsymbol{\omega}_i-\mathbf{Q}_i^T\mathbf{Q}_{i,d}{}^m\boldsymbol{\omega}_{i,d}
\end{aligned}
$$

which are consistent on the $\mathrm{S}_i^2, \mathrm{T}_{q_i}\mathrm{S}_i^2$ manifold error vectors. Their derivatives are calculated by differentiating (14),

$$
\begin{aligned}
{}^m\dot{\mathbf{e}}_{q,i} &= \mathbf{Q}_i^T\Big(({}^b\boldsymbol{\omega}_{i,d}\times{}^b\mathbf{q}_{i,d})\times{}^b\mathbf{q}_i\\
&\quad+{}^b\mathbf{q}_{i,d}\times({}^b\boldsymbol{\omega}_i\times{}^b\mathbf{q}_i)\Big)-S({}^m\boldsymbol{\omega}_i){}^m\mathbf{e}_{q,i} && (15)\\
{}^m\dot{\mathbf{e}}_{\boldsymbol{\omega},i} &= {}^m\dot{\boldsymbol{\omega}}_i+S({}^m\boldsymbol{\omega}_i)\mathbf{Q}_i^T\mathbf{Q}_{i,d}{}^m\boldsymbol{\omega}_{i,d}-\mathbf{Q}_i^T\mathbf{Q}_{i,d}{}^m\dot{\boldsymbol{\omega}}_{i,d}
\end{aligned}
$$

To effectively negotiate the model/sensor inaccuracies while attaining any allocation generated pointing direction, a geometric sliding mode methodology will be employed on S_i^2. The sliding surfaces are constructed in terms of Ψ_i and its associated configuration and velocity errors in order to get a Lyapunov function written in terms of Ψ_i. Then the control design is similar to nonlinear control design in Euclidean spaces. The defined sliding surfaces and their derivatives are,

$$
\begin{aligned}
\mathbf{S}_i &= (\Lambda+\Psi_i){}^m\mathbf{e}_{q,i}+\eta{}^m\mathbf{e}_{\boldsymbol{\omega},i} && (16)\\
\dot{\mathbf{S}}_i &= \dot{\Psi}_i{}^m\mathbf{e}_{q,i}+(\Lambda+\Psi_i){}^m\dot{\mathbf{e}}_{q,i}+\eta{}^m\dot{\mathbf{e}}_{\boldsymbol{\omega},i}
\end{aligned}
$$

where $\Lambda > 0$ and $\eta > 0$ are positive gains. The chosen Lyapunov functions and their derivatives are,

$$\mathbf{V}_i = (\mathbf{S}_i^T\mathbf{S}_i)/2, \dot{\mathbf{V}}_i = \mathbf{S}_i^T\dot{\mathbf{S}}_i$$

To avoid chattering, the convergence of all system trajectories to the sliding surface will be realized by choosing the control ${}^m\mathbf{u}_i$ such that when not on the surface the following holds,

$$\dot{\mathbf{V}}_i = \mathbf{S}_i^T\dot{\mathbf{S}}_i = \sum_{j=1}^3 s_{i,j}\dot{s}_{i,j} \le -\kappa\|\mathbf{S}_i\|^2 \quad (17)$$

where $\kappa>0$ and the subscript $(.)_j$ signifies component wise manipulations. The derived control law is,

$$
\begin{aligned}
{}^m\mathbf{u}_i &= \eta^{-1}\widehat{\mathbf{J}}_p\Big(\eta{}^m\boldsymbol{\alpha}_i-\eta\widehat{\mathbf{f}}_i-\dot{\Psi}_i{}^m\mathbf{e}_{q,i}\\
&\quad-(\Lambda+\Psi_i){}^m\dot{\mathbf{e}}_{q,i}-\gamma\mathbf{S}_i\Big) && (18a)\\
{}^m\boldsymbol{\alpha}_i &= \mathbf{Q}_i^T\mathbf{Q}_{i,d}{}^m\dot{\boldsymbol{\omega}}_{i,d}-S({}^m\boldsymbol{\omega}_i)\mathbf{Q}_i^T\mathbf{Q}_{i,d}{}^m\boldsymbol{\omega}_{i,d} && (18b)\\
\mathbf{f}_i &= \mathbf{J}_p{}^{-1}\left(\mathbf{Q}_i^T({}^b\mathbf{M}_{c,i}+{}^b\mathbf{M}_{p,i})-{}^m\boldsymbol{\omega}_i\times\mathbf{J}_p{}^m\boldsymbol{\omega}_i\right) && (18c)
\end{aligned}
$$

where $\gamma > 0$, while $\widehat{(.)}$ signifies parameter identification errors. Using (18a) and (1b) in (17), after some manipulations,

$$s_{i,j}\dot{s}_{i,j} = -\left(\gamma\frac{(\widehat{\mathbf{J}}_p)_{j,j}}{(\mathbf{J}_p)_{j,j}}s_{i,j}^2-\Upsilon_{i,j}s_{i,j}\right)$$

The above equation is of quadratic form. Analyzing the above equation we see that, for,

$$
\begin{aligned}
|s_{i,j}| &> \frac{|\Upsilon_{i,j}|(\mathbf{J}_p)_{j,j}}{\gamma(\widehat{\mathbf{J}}_p)_{j,j}} \xrightarrow{then} \mathbf{S}_i^T\dot{\mathbf{S}}_i \le -\kappa\|\mathbf{S}_i\|^2 && (19a)\\
\Upsilon_{i,j} &= \left(\mathbf{J}_p^{-1}\widehat{\mathbf{J}}_p-\mathbf{I}\right)_{j,j}\Big(\eta{}^m\boldsymbol{\alpha}_i-(\Lambda+\Psi_i){}^m\dot{\mathbf{e}}_{q,i}\\
&\quad-\dot{\Psi}_i{}^m\mathbf{e}_{q,i}-\eta\widehat{\mathbf{f}}_i\Big)_j+\eta\left(\mathbf{f}_i-\widehat{\mathbf{f}}_i\right)_j && (19b)
\end{aligned}
$$

Observing the above equations, we note that as γ is increased, the trajectories converge faster to the sliding surfaces, while the error boundary around the desired response shrinks. It can be shown that the derived control law is singularity-free, smooth (no high frequency chattering, see Fig. 2(h)), it can handle bounded modeling inaccuracies, and it stabilizes each VA around any given equilibrium except the antipodal equilibrium.

This is the best that can be achieved, since ${}^b\mathbf{q}_{i,d}\times{}^b\mathbf{q}_i$ vanishes at the antipodal equilibrium (almost global). The case were the allocation strategy generates the antipodal equilibrium ${}^b\mathbf{q}_{i,d}=-{}^b\mathbf{q}_i$, which will make the i^{th}-VA stay at ${}^b\mathbf{q}_i$, was studied through extensive simulations which show that, due to the VA's inability to change attitude, an infinitesimal change to the UAVs configuration will take place. Thus in the next control iteration the desired attitude ${}^b\mathbf{q}_{i,d}(t+dt)$ will not be the unstable equilibrium. This case could be triggered also if the allocation strategy receives as command a dramatic change of the UAVs attitude equilibrium. This can be avoided by choosing a proper reference trajectory.

IV. STABILITY ANALYSIS

A stability analysis for the attitude dynamics is developed first, followed by a stability analysis for the position dynamics. A necessary condition for the proofs to hold is that the system lives in $\mathrm{L}_2=\{\mathbf{Q}_d\in\mathrm{SO}(3)|\Psi(\mathbf{Q},\mathbf{Q}_d)<2\}$, meaning, the requested orientation is not antipodal to the current one.

A. Attitude Stability. The attitude error dynamics are calculated by differentiating the attitude component of (7), namely $\mathbf{e}_\omega$. Substituting into the resulting expression (4b), followed by (1b) solved for ${}^m\mathbf{u}_i$, and (3a) to get,

$$
\begin{aligned}
\mathbf{J}\dot{\mathbf{e}}_\omega &= \mathbf{J}\left(S({}^b\boldsymbol{\omega})\mathbf{Q}^T\mathbf{Q}_d{}^b\boldsymbol{\omega}_d-\mathbf{Q}^T\mathbf{Q}_d{}^b\dot{\boldsymbol{\omega}}_d\right)\\
&\quad+\sum_{i=1}^3\Big(\mathbf{A}_i\times\left[\mathbf{Q}^T\mathbf{g}_p-m_p{}^b\dot{\mathbf{v}}_i\right]-\mathbf{Q}_i\mathbf{J}_p\left(\dot{\mathbf{e}}_{\boldsymbol{\omega},i}+{}^m\boldsymbol{\alpha}_i\right)\\
&\quad-\mathbf{Q}_i({}^m\boldsymbol{\omega}_i\times\mathbf{J}_p{}^m\boldsymbol{\omega}_i)\Big)+\mathbf{A}_M[{}^b\mathbf{F}_{p,1};{}^b\mathbf{F}_{p,2};{}^b\mathbf{F}_{p,3}]\\
&\quad+\mathbf{J}{}^b\boldsymbol{\omega}\times{}^b\boldsymbol{\omega}+{}^b\mathbf{M}_D && (20)
\end{aligned}
$$

Substituting ${}^b\mathbf{F}_{p,i} = {}^b\mathbf{F}_{p,i_d}+{}^b\mathbf{F}^e_{p,i}$ to (20) and the attitude component of (8) we get,

$$
\begin{aligned}
\mathbf{J}\dot{\mathbf{e}}_\omega &= {}^b\dot{\boldsymbol{\omega}}_r+\sum_{i=1}^3\Big(-\mathbf{Q}_i\mathbf{J}_p\dot{\mathbf{e}}_{\boldsymbol{\omega},i}+\mathbf{A}_i\times\left[-m_p{}^b\dot{\mathbf{v}}_i\right]\Big) && (21)\\
&\quad+\mathbf{A}_M[{}^b\mathbf{F}^e_{p,1};{}^b\mathbf{F}^e_{p,2};{}^b\mathbf{F}^e_{p,3}]+{}^b\mathbf{M}_D
\end{aligned}
$$

The final form of the attitude error dynamics is,

$$
\begin{aligned}
\mathbf{J}\dot{\mathbf{e}}_\omega &= -k_R\mathbf{e}_Q-k_\Omega\mathbf{e}_\omega-c_2k_Q\mathbf{e}_Q-k_\omega\mathbf{e}_\omega+\boldsymbol{\epsilon}_Q && (22)\\
\boldsymbol{\epsilon}_Q &= \sum_{i=1}^3\Big(\mathbf{A}_i\times\left[-m_p{}^b\dot{\mathbf{v}}_i\right]-\mathbf{Q}_i\mathbf{J}_p\dot{\mathbf{e}}_{\boldsymbol{\omega},i}\Big)\\
&\quad+\mathbf{A}_M[{}^b\mathbf{F}^e_{p,1};{}^b\mathbf{F}^e_{p,2};{}^b\mathbf{F}^e_{p,3}]+{}^b\mathbf{M}_D
\end{aligned}
$$

where $\boldsymbol{\epsilon}_Q$ is the attitude disturbance term that includes VA tracking errors, wind disturbances and VA related accelerations (${}^b\dot{\mathbf{v}}_i$) see (A2). Due to the small mass/inertia properties of the VA these are dealt as disturbances. Our choice of attitude/angular velocity tracking errors dictates a Lyapunov function as in [8], with $c_2 > 0$,

$$V_Q = (\mathbf{e}_\omega\cdot\mathbf{J}\mathbf{e}_\omega)/2+k_R\Psi(\mathbf{Q},\mathbf{Q}_d)+c_2\mathbf{e}_\omega\cdot\mathbf{e}_Q \quad (23)$$

It can be shown that the following inequality holds (see [8]),

$$\lambda_{min}(W_{11})\|z\|^2 \leqq V_Q \leqq \lambda_{max}(W_{12})\|z\|^2 \quad (24)$$

where $z=[\|\mathbf{e}_Q\|;\|\mathbf{e}_\omega\|]\in\mathbb{R}^2$ and W_{11}, W_{12} are given by, $W_{11}=\frac{1}{2}\begin{bmatrix}2k_R & c_2\\ c_2 & \lambda_{min}(\mathbf{J})\end{bmatrix}, W_{12}=\begin{bmatrix}2k_R & \frac{1}{2}c_2\\ \frac{1}{2}c_2 & \frac{1}{2}\lambda_{max}(\mathbf{J})\end{bmatrix}$

Our work focuses on the derivative of the Lyapunov function where the UAV dynamics appear. After a considerable amount of manipulations,

$$\begin{aligned}\dot V_Q &= \mathbf{e}_\omega\cdot\mathbf{J}\dot{\mathbf{e}}_\omega + k_R\mathbf{e}_\omega\cdot\mathbf{e}_Q + c_2\dot{\mathbf{e}}_\omega\cdot\mathbf{e}_Q + c_2\mathbf{e}_\omega\cdot\dot{\mathbf{e}}_Q\\ &\leqq -z^TW_{13}z + (\frac{1}{4k_\omega}+\frac{\lambda_{max}(\mathbf{J})}{4k_Q(\lambda_{min}(\mathbf{J}))^2})\|\boldsymbol{\epsilon}_Q\|^2\\ &\quad -\frac{c_2^2k_Q}{\lambda_{max}(\mathbf{J})}(\|\mathbf{e}_Q\|-\frac{\lambda_{max}(\mathbf{J})}{2c_2k_Q\lambda_{min}(\mathbf{J})}\|\boldsymbol{\epsilon}_Q\|)^2\\ &\quad -k_\omega(\|\mathbf{e}_\omega\|-\|\boldsymbol{\epsilon}_Q\|/2k_\omega)^2 \end{aligned}\tag{25}$$

$$W_{13}=\begin{bmatrix}\frac{c_2k_R}{\lambda_{max}(\mathbf{J})} & -\frac{c_2}{2}(\frac{k_\Omega+k_\omega}{\lambda_{min}(\mathbf{J})}+k_Q)\\ -\frac{c_2}{2}(\frac{k_\Omega+k_\omega}{\lambda_{min}(\mathbf{J})}+k_Q) & k_\Omega-\frac{c_2}{2}\end{bmatrix}$$

Arriving at the inequality,

$$\dot V_Q \leqq -\lambda_{min}(W_{13})\|z\|^2+(\frac{1}{4k_\omega}+\frac{\lambda_{max}(\mathbf{J})}{4k_Q(\lambda_{min}(\mathbf{J}))^2})\|\boldsymbol{\epsilon}_Q\|^2$$

$$c_2<min\Big\{2k_\Omega,\sqrt{2k_R\lambda_{min}(\mathbf{J})},\frac{k_Rk_\Omega}{\lambda_{max}(\mathbf{J})\left(\frac{k_R}{2\lambda_{max}(\mathbf{J})}+\frac{1}{4}(\frac{k_\Omega+k_\omega}{\lambda_{min}(\mathbf{J})}+k_Q)^2\right)}\Big\}\tag{26}$$

and W_{11}, W_{12}, W_{13} are positive definite. Furthermore, the following inequality holds for $\lambda_Q{=}\lambda_{min}(W_{13})/\lambda_{max}(W_{12})$,

$$\dot V_Q \leqq -\lambda_Q V_Q+\phi_Q\tag{27a}$$

$$\phi_Q=(\frac{1}{4k_\omega}+\frac{\lambda_{max}(\mathbf{J})}{4k_Q(\lambda_{min}(\mathbf{J}))^2})\|\boldsymbol{\epsilon}_Q\|^2_{max}\tag{27b}$$

Boundedness: Utilizing (24), (27a), if the states are in, $\mathrm{L}_n=\{(\mathbf{Q},{}^b\boldsymbol{\omega})\in\mathrm{SO}(3)\times\mathbb{R}^3|\|z\|>\sqrt{\phi_Q/\lambda_{min}(W_{13})}\}$ then $\dot V_Q<0$. For initial conditions in $\mathrm{L}_\delta=\{(\mathbf{Q},{}^b\boldsymbol{\omega})\in\mathrm{SO}(3)\times\mathbb{R}^3|V_Q<\lambda_{min}(W_{11})\}$ then $\mathrm{L}_\delta\subseteq\mathrm{L}_2$. Finally for,

$$\phi_Q<(\lambda_{min}(W_{11})\lambda_{min}(W_{13}))/\lambda_{max}(W_{12})\tag{28}$$

then $\mathrm{L}_n^c{\subset}\mathrm{L}_\delta{\subseteq}\mathrm{L}_2$ and the attitude errors exponentially converge to L_n^c and are uniformly ultimately bounded. The superscript $(.)^c$ denotes the complement set of (.). The estimated ultimate bound is,

$$\|z\|^2\le\frac{\lambda_{max}(W_{12})}{\lambda_{min}(W_{11})\lambda_{min}(W_{13})}\phi_Q$$

Condition (28) is required to ensure that $\mathrm{L}_n^c{\subset}\mathrm{L}_\delta$ and the disturbance term is small enough such that the states remain in $\mathrm{L}_\delta{\subseteq}\mathrm{L}_2$. L_n^c can be reduced by increasing the k_ω, k_Q gains.

B. Position Stability. The position error dynamics are calculated by substituting ${}^b\mathbf{F}_{p,i}{=}{}^b\mathbf{F}_{p,i_d}{+}{}^b\mathbf{F}^e_{p,i}$ in (3a), where ${}^b\mathbf{F}^e_{p,i}$ is the thrust tracking error, and the resulting expression in (4a) followed by the position component of (8) to get,

$$m_b\dot{\mathbf{v}}=m_b\dot{\mathbf{v}}_r+\mathbf{Q}(\sum\nolimits_{i=1}^3({}^b\mathbf{F}^e_{p,i}-m_p{}^b\dot{\mathbf{v}}_i)+{}^b\mathbf{F}_D)\tag{29}$$

Substituting for the reference trajectory term from (9),

$$\dot{\mathbf{e}}_v=-k_v\mathbf{e}_v-c_xk_x\mathbf{e}_x+\boldsymbol{\epsilon}_x/m_b\tag{30}$$

$$\boldsymbol{\epsilon}_x=\mathbf{Q}\big(\mathbf{A}_F[{}^b\mathbf{F}^e_{p,1};{}^b\mathbf{F}^e_{p,2};{}^b\mathbf{F}^e_{p,3}]+{}^b\mathbf{F}_D+\sum\nolimits_{i=1}^3\left(-m_p{}^b\dot{\mathbf{v}}_i\right)\big)$$

where $\boldsymbol{\epsilon}_x$ is the position disturbance term that includes VA tracking errors, wind disturbances and VA related accelerations (${}^b\dot{\mathbf{v}}_i$) see (A2), that due to the small mass/inertia properties of the VA, are dealt as disturbances. The following Lyapunov function is employed, with $c_x>0$,

$$V_x=\frac{1}{2}\|\mathbf{e}_v\|^2+\frac{1}{2}c_xk_xk_v\|\mathbf{e}_x\|^2+c_x\mathbf{e}_x\cdot\mathbf{e}_v\tag{31}$$

and for $z_x{=}[\|\mathbf{e}_x\|;\|\mathbf{e}_v\|]{\in}\mathbb{R}^2$ the following inequality holds,

$$\lambda_{min}(\Pi_{11})\|z_x\|^2\leqq V_x\leqq\lambda_{max}(\Pi_{12})\|z_x\|^2\tag{32}$$

$$\Pi_{11}=\frac{1}{2}\begin{bmatrix}c_xk_xk_v & -c_x\\ -c_x & 1\end{bmatrix},\ \Pi_{12}=\frac{1}{2}\begin{bmatrix}c_xk_xk_v & c_x\\ c_x & 1\end{bmatrix}$$

where $\lambda_{min,max}(.)$ denotes the min, max eigenvalue of (.). Differentiating (31), substituting (30), $k_v=k_\tau+k_\mu$ and $k_x=k_\xi+k_\lambda$ to the resulting equation ($k_\tau,k_\mu,k_\xi,k_\lambda>0$), after considerable manipulations, we arrive at the inequality,

$$\begin{aligned}\dot V_x &\leqq -z_x^T\Pi_{13}z_x+\frac{1}{4}\left(\frac{k_\mu+k_\lambda}{m_b^2k_\lambda k_\mu}\right)\|\boldsymbol{\epsilon}_x\|^2 &(33a)\\ &\quad -k_\mu(\|\mathbf{e}_v\|-\frac{\|\boldsymbol{\epsilon}_x\|}{2k_\mu m_b})^2-c_x^2k_\lambda(\|\mathbf{e}_x\|-\frac{\|\boldsymbol{\epsilon}_x\|}{2c_xk_\lambda m_b})^2\\ &\leqq -\lambda_{min}(\Pi_{13})\|z_x\|^2+\frac{k_\mu+k_\lambda}{4m_b^2k_\lambda k_\mu}\|\boldsymbol{\epsilon}_x\|^2_{max} &(33b)\end{aligned}$$

$$\Pi_{13}=\begin{bmatrix}c_xk_\xi & -\frac{1}{2}c_x(k_xk_v-k_x-k_v)\\ -\frac{1}{2}c_x(k_xk_v-k_x-k_v) & k_\tau-c_x\end{bmatrix}$$

$$c_x<min\Big\{k_\tau,\sqrt{k_xk_v},\frac{4k_\xi k_\tau}{4k_\xi+(k_vk_x-k_x-k_v)^2}\Big\}\tag{34}$$

and $\Pi_{11},\Pi_{12},\Pi_{13}$ are positive definite. Furthermore, the following inequality holds for $\lambda_x=\lambda_{min}(\Pi_{13})/\lambda_{max}(\Pi_{12})$,

$$\dot V_x\leqq-\lambda_xV_x+\phi_x,\phi_x{=}\frac{k_\mu+k_\lambda}{4m_b^2k_\lambda k_\mu}\|\boldsymbol{\epsilon}_x\|^2_{max}\tag{35}$$

Boundedness: Using (32), (33b), if the system evolves in $\mathrm{L}_k{=}\{(\mathbf{e}_x,\mathbf{e}_v){\in}\mathbb{R}^3{\times}\mathbb{R}^3|\|z_x\|{>}\sqrt{\phi_x/\lambda_{min}(\Pi_{13})}\}$ then $\dot V_x{<}0$. For initial conditions in $\mathrm{L}_\beta=\{(\mathbf{Q},{}^b\boldsymbol{\omega},\mathbf{e}_x,\mathbf{e}_v)\in\mathrm{SO}(3)\times\mathbb{R}^3\times\mathbb{R}^3\times\mathbb{R}^3|V_x<\lambda_{min}(\Pi_{11})e_{x_{max}},V_Q<\lambda_{min}(W_{11})\}$ where $\|\mathbf{e}_x(0)\|^2{\le}e_{x_{max}}{\in}\mathbb{R}$ then the solution is also in $\{\mathrm{L}_\delta\subseteq\mathrm{L}_2\}$. Finally for,

$$\phi_x<(\lambda_{min}(\Pi_{11})\lambda_{min}(\Pi_{13})e_{x_{max}})/\lambda_{max}(\Pi_{12})\tag{36}$$

then $\mathrm{L}_k^c{\subset}\mathrm{L}_\beta$ and $\mathbf{e}_x,\mathbf{e}_v$ exponentially converge to L_k^c and are uniformly ultimately bounded. The ultimate bound is,

$$\|z_x\|^2\le\frac{\lambda_{max}(\Pi_{12})}{\lambda_{min}(\Pi_{11})\lambda_{min}(\Pi_{13})}\phi_x$$

Condition (36) is required to ensure that $\mathrm{L}_k^c{\subset}\mathrm{L}_\beta$ and the disturbance term is small enough such that the states do not exit L_β. L_k^c can be reduced by increasing the k_λ,k_μ gains.

C. System Position/Attitude Stability. A Lypunov function for the complete system is,

$$\lambda_o\|z_c\|^2\leqq\{V{=}V_x+V_Q\}\leqq\lambda_M\|z_c\|^2\tag{37}$$

$$\lambda_o=\min\{\lambda_{min}(\Pi_{11}),\lambda_{min}(W_{11})\}$$

$$\lambda_M=\max\{\lambda_{max}(\Pi_{12}),\lambda_{max}(W_{12})\}$$

where $z_c{=}[z_x;z]$. Its derivative is given by,

$$\begin{aligned}\dot V &\leqq -\lambda_xV_x-\lambda_QV_Q+\phi\\ &\leqq -\lambda_mV+\phi,\ \lambda_m=\min\{\lambda_x,\lambda_Q\}\end{aligned}\tag{38}$$

where $\phi=\phi_x+\phi_Q$. Applying the comparison Lemma [13],

$$V(t)\leqq V(0)e^{-\lambda_mt}+\phi/\lambda_m\tag{39}$$

$$\|z_c(t)\|\leqq\sqrt{\lambda_M/\lambda_o}\|z_c(0)\|e^{-\frac{\lambda_m}{2}t}+\sqrt{\phi/(\lambda_o\lambda_m)}\tag{40}$$

Boundedness: Using (37), (38), if the system evolves in $\mathrm{L}_\eta = \{(\mathbf{Q}, {}^b\boldsymbol{\omega}, \mathbf{x}, \mathbf{v}) \in \mathrm{SO}(3) \times \mathbb{R}^3 \times \mathbb{R}^3 \times \mathbb{R}^3 | \|z_c\| > \sqrt{\phi/\lambda_m \lambda_o}\}$ then $\dot{V} < 0$. For initial conditions in $\mathrm{L}_s = \{(\mathbf{Q}, {}^b\boldsymbol{\omega}, \mathbf{x}, \mathbf{v}) \in \mathrm{SO}(3) \times \mathbb{R}^3 \times \mathbb{R}^3 \times \mathbb{R}^3 | V < \lambda_o(1 + e_{x_{max}})\}$ then the solution is also in L_β. Finally for,

$$\phi < \lambda_m \lambda_o (1 + e_{x_{max}}) \tag{41}$$

then $\mathrm{L}_\eta^c \subset \mathrm{L}_s$ and $\mathbf{e}_Q, \mathbf{e}_\omega, \mathbf{e}_x, \mathbf{e}_v$ exponentially converge to L_η^c and are uniformly ultimately bounded. The estimated ultimate bound is,

$$\|z_c\|^2 \leq \phi/\lambda_o \lambda_m$$

Condition (41) ensures that $\mathrm{L}_\eta^c \subset \mathrm{L}_s$ and that the disturbance terms are small enough such that the states remain bounded within L_s. L_η^c can be reduced by increasing the $k_Q, k_\omega, k_\lambda, k_\mu$ gains.

V. SIMULATION RESULTS

The effectiveness of the proposed strategy is verified through simulations. The system parameters are:

$$^b\mathbf{p}_1 = [0.1940; -0.1120; 0][m], {}^b\mathbf{p}_2 = [0; 0.2240; 0][m]$$

$$^b\mathbf{p}_3 = [-0.1940; -0.1120; 0][m]$$

$$b_F = 3.409 \cdot 10^{-4}[N\,(s/rad)^2], b_T = 7.444 \cdot 10^{-3}[m]$$

$$d = 0.014[m], m_b = 1[kg], m_p = 0.060[kg]$$

$$\mathbf{J} = diag(0.0205, 0.0211, 0.0344)[kgm^2]$$

$$\mathbf{J}_p = diag(0.1341, 0.1341, 0.0919) \cdot 10^{-4}[kgm^2]$$

The controller parameters are chosen to satisfy (26), (34). A preliminary estimate is calculated first through pole placement by choosing desired time constants coefficients:

$$k_R + k_Q = diag(2.1938, 2.2607, 3.6840) \in \mathbb{R}^{3\times3}$$

$$k_\omega + k_\Omega = diag(0.4241, 0.4371, 0.7122) \in \mathbb{R}^{3\times3}$$

$$k_x = 100, k_v = 20, \gamma = 144, \Lambda = 360000, \eta = 1200$$

A complex flight maneuver for which the UAV firstly recovers from being upside down and then follows a desired pose trajectory will be carried out. The initial conditions are

$$\mathbf{x}(0) = [-1; -1; 0][m],\ \mathbf{Q}(0) = \mathbf{Q}_r\,(0, 179^o, 0)\,,\ \mathbf{Q}_i(0) = \mathbf{I}$$

$$\mathbf{v}(0) = [0;0;0][m], \boldsymbol{\omega}(0) = \boldsymbol{\omega}_i(0) = [0;0;0][rad/s], i = 1, 2, 3$$

$\mathbf{Q}_r(t)$ is given in the Appendix. The trajectory in $\mathbf{E}^3$ is that of an "8", while attitude wise the UAV performs a 360^o roll maneuver. Analytically,

$$\mathbf{x}_d(t) = [sin(0.03t); sin(0.06t); 2][m], \mathbf{Q}_d(t) = \mathbf{Q}_r(0, \frac{\pi t}{105}, 0)$$

To demonstrate the effectiveness of the controller, the simulation includes parameter errors:

$$\widehat{b}_F = b_F + 0.033 b_F, \widehat{b}_T = b_T + 0.033 b_T, \widehat{d} = d + 0.01 d$$

$$\widehat{m}_b = m_b + 0.01 m_b, \widehat{m}_p = m_p + 0.33 m_p, \widehat{\mathbf{J}}_p = \mathbf{J}_p + 0.33 \mathbf{J}_p$$

A bounded disturbance wrench $[{}^b\mathbf{F}_D; {}^b\mathbf{M}_D]$ simulating the wind under "fresh breeze" conditions (17-21(Knots)) is applied according to [11].

Because the desired trajectory begins at $\mathbf{x}_d(0) = [0; 0; 2]$[m] and the UAV is upside down, there is a large initial position and attitude errors, $\|\mathbf{e}_x\|$=2.4595[m] and Ψ=1.9825 (179^o in terms of the roll angle), respectively (see Fig. 2(a,b)). The time scale in Fig. 2(a,b) is uneven in order to show both the transient and steady state response. The UAV recovers in 1s, Fig. 2(a,b), and starts to track the figure "8" trajectory, Fig. 2(c), while performing a 360^o rotation around the $\mathbf{e}_1$ body fixed axis. Fig. 2(a,b) also includes an enlarged view of the last 50s of the simulation to highlight the results. The tracking performance is shown in both Fig. 2(a,b) maintaining the position error below $\|\mathbf{e}_x\|$<0.02[m] and the attitude error below $\Psi < 1 \cdot 10^{-4}$ which is less than 0.009[deg] with respect to an equivalent axis angle rotation.

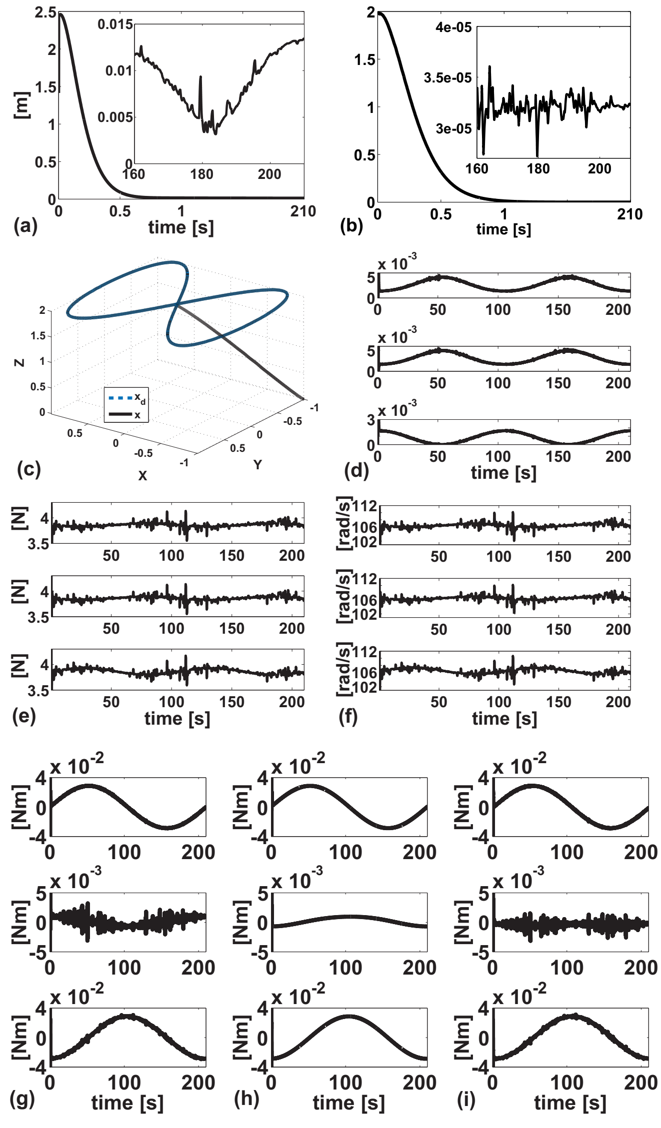

Fig. 2. Pose tracking (a) Normed position error $\|\mathbf{e}_x\|$. (b) Attitude error Ψ. (c) Figure "8" trajectory (blue: desired, black: actual). (d) Attitude difference between thrusting motors using Ψ_i (top: 1^{st} wrt 3^{rd}, middle: 2^{nd} wrt 3^{rd}, bottom: 1^{st} wrt 2^{nd}). (e) Propeller thrusts (top: f_1, middle: f_2, bottom: f_3, (N)). (f) Propeller speed (top: $^m\boldsymbol{\omega}_{1,3}$, middle: $^m\boldsymbol{\omega}_{2,3}$, bottom: $^m\boldsymbol{\omega}_{3,3}$, (rad/s)). (g) Control torque $^m\mathbf{u}_1$ (left column, each component, (Nm)). (h) Control torque $^m\mathbf{u}_2$ (middle column, each component, (Nm)). (i) Control torque $^m\mathbf{u}_3$ (right column, each component, (Nm))

The VAs are operating in cooperative manner since they show small relative attitude difference wrt each other Ψ_i<0.006, see Fig. 2(d), which is less than 0.54[deg] with respect to an equivalent axis angle rotation. This is attributed to the pseudoinverse allocation strategy. The propeller thrusts shown in Fig. 2(e) verify that the UAV can overcome gravity while in Fig. 2(f) the propeller speeds can be seen. The vectoring gains generate realistic and realizable control torques that can be seen in Fig. 2(g,h,i). The same simulation but without wind was executed to investigate the behavior of the vectoring controller, with the generated second VA control torques shown in Fig. 2(h). This figure shows that the spikes in Fig. 2(g,i) were due to the wind disturbance verifying the claim that the vectoring controller is smooth, without high frequency chattering.

The vectoring of the motors can be implemented using two gimbals, one mounted on the other with orthogonal pivot axes, avoiding limitations of the actuation apparatus such as finite range for the tilting angles. The advantages gained by utilizing geometric control methodologies lie in that we do not have to worry about critical orientations for the VAs or the base that might arise during operation.

Despite modeling inaccuracies of up to 33% for some parameters and disturbances, the system successfully tracks the desired pose trajectory with independent control over its attitude/translational dynamics (holonomic response) verifying that the UAV can hover and maneuver at any attitude without restrictions.

VI. CONCLUSIONS

The modeling and control of a vectoring tricopter UAV were addressed in this article. The UAV is actuated by three thrust motors, each guided by suitable actuators, forming a platform able to independently track any desired attitude and trajectory. The derivation of the equations of motion was followed by the development of a singularity-free control strategy based on geometric feedback linearization that accounts for the inertial effects of the main body, the motors and of the vectoring actuators. A stability proof was provided. Simulations verified the effectiveness of the tricopter configuration and the developed control design, demonstrating a UAV with independent control over its attitude/translational dynamics and a global operational envelope. Future work includes, the development of a prototype and the experimental implementation of the proposed strategy.

REFERENCES

[1] T. Lee, M. Leok, and N. McClamroch, "Geometric tracking control of a Quadrotor UAV on SE(3)," arXiv:1003.2005v1. [Online]. Available: http://arxiv.org/abs/1003.2005v1

[2] Lindsey, Q., Mellinger, D., and Kumar, V., "Constraction of Cubic Structures with Quadrotor Teams," *Proceedings of Robotics: Science and Systems*, June 27 - June 30, Los Angeles, California, USA, 2011.

[3] H. Romero *et al.*, "Modelling and real-time control stabilization of a new VTOL aircraft with eight rotors," in *Proc. of the 2007 International Conference on Intelligent Robots and Systems (IROS '07)*, San Diego, CA, USA, October 2007, pp. 147-152.

[4] Richard Voyles and Guangying Jiang, "Hexrotor UAV platform enabling dextrous interaction with structures-flight test," *IEEE International Symposium on Safety, Security, and Rescue Robotics (SSRR '13)*, Oct 21-26 2013, Linkoping, Sweden.

[5] B. Crowther *et al.*, "Kinematic Analysis and Control Design for a Nonplanar Multirotor Vehicle," *J. of Guidance, Control, and Dynamics*, Vol. 34, No. 4 (2011), pp. 1157-1171.

[6] Markus Ryll, Heinrich H. Blthoff, Paolo Robuffo Giordano, "First flight tests for a quadrotor UAV with tilting propellers," *IEEE International Conference on Robotics and Automation (ICRA '13)*, May 6-10 2013, Karlsruhe, Germany, pp. 295-302.

[7] N. A. Chaturvedi, A. K. Sanyal, and N. H. McClamroch, "Rigid-Body Attitude Control Using Rotation Matrices For Continuous, Singularity-Free Control Laws," *IEEE Control Systems Magazine*, Vol. 31, No. 3, June. 2011, pp. 30-51.

[8] T. Lee, "Geometric Tracking Control of the Attitude Dynamics of a Rigid Body on $SO(3)$," in *Proceeding of the American Control Conference*, 2011, pp. 1885-1891.

[9] T. Lee, M. Leok, and N. McClamroch, "Stable Manifolds of saddle equilibria for pendulum dynamics on S^2 and $SO(3)$," in *IEEE Conference on Decision and Control and European Control Conference*, December 2011, pp. 3915-3921.

[10] A. Tayebi and S. McGilvray, "Attitude stabilization of a VTOL quadrotor aircraft," *IEEE Transactions on Control System Technology*, vol. 14, no. 3, 2006, pp. 562-571.

[11] Thor I. Fossen, *Handbook of Marine Craft Hydrodynamics and Motion Control*, First Edition, 2011, John Wiley & Sons Ltd.

[12] Ramp, M. and Papadopoulos, E., "Attitude and Angular Velocity Tracking for a Rigid Body using Geometric Methods on the Two-Sphere," *Proc. of the European Control Conference 2015*, Johannes Kepler University, Linz, Austria, July 15-17, 2015.

[13] Hassan K. Khalil, *Nonlinear Systems*, 3rd Edition, Prentice Hall, 2002.

[14] F. Bullo and A. Lewis, *Geometric control of mechanical systems.*, Springer-Verlag, 2005.

APPENDIX

The attitude error function as given by, [8],

$$\Psi(t) = 2 - \sqrt{1 + tr[\mathbf{Q}_d^T \mathbf{Q}]} \tag{A1}$$

Angular velocity and acceleration of the CM of the i^{th}VA,

$$\begin{gathered} {}^m\boldsymbol{\omega}_i = {}^m\boldsymbol{\omega}_i^r + \mathbf{Q}_i^T {}^b\boldsymbol{\omega} \\ {}^b\dot{\mathbf{v}}_i = \mathbf{Q}^T\dot{\mathbf{v}} + {}^b\dot{\mathbf{v}}_i^r \\ {}^b\dot{\mathbf{v}}_i^r = \mathbf{Q}^T(\ddot{\mathbf{Q}}({}^b\mathbf{p}_i + \mathbf{Q}_i{}^m\mathbf{p}) + 2\dot{\mathbf{Q}}(\dot{\mathbf{Q}}_i{}^m\mathbf{p}) + \mathbf{Q}(\ddot{\mathbf{Q}}_i{}^m\mathbf{p})) \end{gathered} \tag{A2}$$

Vector space isomorphism where $\mathbf{r} \in \mathbb{R}^3$,

$$\begin{gathered} S(\mathbf{r}) = [0, -r_3, r_2; r_3, 0, -r_1; -r_2, r_1, 0] \\ S^{-1}(S(\mathbf{r})) = \mathbf{r} \end{gathered} \tag{A3}$$

Attitude through Euler-Angles ($c\gamma_i = \cos\gamma_i$, $s\gamma_i = \sin\gamma_i$),

$$\mathbf{Q}_r = \begin{bmatrix} 1 & 0 & 0 \\ 0 & c\gamma_1 & s\gamma_1 \\ 0 & -s\gamma_1 & c\gamma_1 \end{bmatrix} \begin{bmatrix} c\gamma_2 & 0 & -s\gamma_2 \\ 0 & 1 & 0 \\ s\gamma_2 & 0 & c\gamma_2 \end{bmatrix} \begin{bmatrix} c\gamma_3 & s\gamma_3 & 0 \\ -s\gamma_3 & c\gamma_3 & 0 \\ 0 & 0 & 1 \end{bmatrix} \tag{A4}$$

Matrix $\mathbb{M} \in \mathbb{R}^{15\times15}$, from (5), where $M_{i,j} \in \mathbb{R}^{3\times3}$,

$$\mathbb{M} = \begin{bmatrix} M_{1,1} & M_{1,2} & M_{1,3} & M_{1,4} & M_{1,5} \\ M_{2,1} & M_{2,2} & M_{2,3} & M_{2,4} & M_{2,5} \\ M_{3,1} & M_{3,2} & M_{3,3} & 0 & 0 \\ M_{4,1} & M_{4,2} & 0 & M_{4,4} & 0 \\ M_{5,1} & M_{5,2} & 0 & 0 & M_{5,5} \end{bmatrix} \tag{A5}$$

$$M_{1,1} = (m_b + 3m_p)\mathbf{I}, M_{1,2} = -\mathbf{Q}\sum_{i=1}^{3} S({}^b\mathbf{p}_i + \mathbf{Q}_i{}^m\mathbf{p})$$

$$M_{1,i} = -\mathbf{Q}\mathbf{Q}_i S({}^m\mathbf{p}), i = 3-5, M_{2,1} = \sum_{i=1}^{3} S({}^b\mathbf{p}_i) m_p \mathbf{Q}^T$$

$$M_{2,2} = \mathbf{J} - \sum_{i=1}^{3} S({}^b\mathbf{p}_i) m_p S({}^b\mathbf{p}_i + \mathbf{Q}_i{}^m\mathbf{p})$$

$$M_{2,i} = -S({}^b\mathbf{p}_i) m_p \mathbf{Q}_i S({}^m\mathbf{p}), i = 3-5$$

$$M_{i,1} = \mathbf{Q}_i^T S(\mathbf{Q}_i({}^m\mathbf{p})) m_p \mathbf{Q}^T, i = 3-5$$

$$M_{i,2} = \mathbf{Q}_i^T S(\mathbf{Q}_i(-{}^m\mathbf{p})) m_p S({}^b\mathbf{p}_i + \mathbf{Q}_i{}^m\mathbf{p}), i = 3-5$$

$$M_{i,i} = \mathbf{J}_p + \mathbf{Q}_i^T S(\mathbf{Q}_i(-{}^m\mathbf{p})) m_p \mathbf{Q}_i S({}^m\mathbf{p}), i = 3-5$$